Earth and Planetary Science Letters 411 (2015) 37–44

Contents lists available at ScienceDirect

Earth and Planetary Science Letters

www.elsevier.com/locate/epsl

A numerical approach to melting in warm subduction zones

Pierre Bouilhol *, Valentina Magni, Jeroen van Hunen, Lars Kaislaniemi

Department of Earth Sciences, Durham University, Science Labs, Durham DH13LE, United Kingdom

ARTICLE INFO

Article history:
Received 28 May 2014
Received in revised form 14 November 2014
Accepted 25 November 2014
Available online 12 December 2014
Editor: J. Brodholt

Keywords:
slab melting
slab dehydration
mantle wedge melting
modeling
thermodynamics

ABSTRACT

The complex feedback between dehydration and melting in hot subduction zones is quantitatively addressed in this study. We present an integrated numerical tool that combines a high-resolution thermo-mechanical subduction model with a thermodynamic database that allows modeling metamorphic devolatilization, and subsequent re-hydration and melting reactions. We apply this tool to quantify how the hydration state of a lithologically layered subducting slab varies during interaction with the hot mantle wedge and how this affects any melting taking place in the subducting crust or the overlying mantle wedge. Total crustal dehydration is achieved before any crustal melting can occur, even in very young subducting slabs. Significant oceanic crust melting is only achieved if the metamorphic fluids from the dehydrating underlying subducting slab mantle are fluxed through the dry eclogites. But our models further demonstrate that even if the oceanic crust can melt in these specific conditions, the preceding crustal dehydration will simultaneously result in extensive mantle wedge melting at lower pressures than for colder slabs. The significant mantle wedge melting implies that also for hot subduction zones, most of the melt feeding the overriding plate is of mantle origin.

1. Introduction

Subduction zones are part of the geochemical cycle for volatiles, and are an essential site for the production of silica-rich magmas that contribute to the formation of continental crust (e.g. Arculus, 1981; Taylor and McLennan, 1995). Modern subduction zone magmatic processes are mainly driven by slab devolatilization that triggers flux melting of the metasomatized mantle wedge and strongly influences the geochemical characteristics of arc magmatism (Tatsumi and Kogiso, 1997; Ulmer, 2001). It is within the arc crust that most silicic-rich granitoids are formed, either by fractional crystallization of mantle wedge primitive parental melts, or, alternatively, by re-melting of previously crystallized primitive melts. But in an unusually warm subduction regime, e.g. in a young slab, water-present melting (water saturated melting) or water-absent melting (dehydration melting) of slab crust may take place, producing Na–Al rich dacitic melts, with high Sr/Y and La/Yb ratios (symptomatic of the presence of garnet and/or amphibole), commonly known as adakites (Moyen, 2009). This process has also been suggested to be at the origin of the early Earth's crust (e.g. Martin, 1999). High-Mg andesites with specific trace element ratios originally recognized in the Adak island of the Aleutian Arc (Kay, 1978) were subsequently termed adakites when interpreted to be slab melts. This terminology arose from Defant and Drummond (1990), who recognized that adakitic compositions from the Austral Andes are related to the subduction of a young (<25-Myr old) oceanic plate. But a considerable debate exists about the processes leading to an adakitic signature: in addition to mafic crust melting as a means to produce adakites (Rapp et al., 1991; Atherton and Petford, 1993), high pressure fractionation of water rich mantle melts also generates "adakitic" compositions (Macpherson et al., 2006; Alonso-Perez et al., 2009), as does the interaction between mantle wedge peridotite and slab partial melts (Rapp et al., 1999). This study intends to better constrain the possible source of an adakitic signal during the subduction of a young lithosphere and provide a better understanding of the magmatic outcome of a warm subduction zone.

Because the effect of metamorphic fluid advection has long been recognized as the primary factor for the generation of subduction zone magmas (Ringwood, 1974), significant effort has been put into constraining the distribution of water distilled from the descending slab. This has been widely investigated experimentally (e.g. Ulmer and Trommsdorff, 1995; Schmidt and Poli, 1998; Grove et al., 2006) and numerically (e.g. Iwamori, 1998; Rüpke et al., 2004; Arcay et al., 2005; Connolly, 2005; Hacker, 2008; Wada et al., 2012; Magni et al., 2014). Numerical models have simulated slab dehydration in warm regimes (Syracuse et al., 2010; van Keken et al., 2011; Magni et al., 2014), but much less attention has been given to the melting processes and the magmatic outcome in these systems.

* Corresponding author. Tel.: +44 (0) 191 33 42356.
E-mail address: pierre.bouilhol@durham.ac.uk (P. Bouilhol).

http://dx.doi.org/10.1016/j.epsl.2014.11.043

In this study, we use a numerical model that reproduces the thermo-mechanical essential characteristics of a subducting slab and computes the thermodynamic equilibrium parageneses at each pressure–temperature–composition (P–T–X) condition of the system at every time step. The resulting paragenetic map of a subduction system allows us to quantify the fate of water during dehydration and subsequent re-hydration or melting reactions. This study has two main objectives: (1) to model these processes envisioned to occur in an ordinary subduction zone, by examining a 40-Myr old subducting slab; and (2) to quantify the dehydration process and the occurrence of melting in a much hotter subduction zone. We show that oceanic crust melting can only be achieved if free water is supplied by dehydration reactions occurring deeper in the slab, but that extensive mantle wedge melting is still the main overriding plate supplier.

2. A dynamic solidus setup

We have developed a numerical tool that unifies a thermo-mechanical finite element model with a thermodynamic database, which allows us to model phase assemblages and the metamorphic evolution of a lithologically layered slab of a subduction zone system.

2.1. Combined thermo-chemical–mechanical model

We use the finite element code Citcom to calculate the flow field and temperature distribution inside a subduction system in a Cartesian geometry (Moresi and Gurnis, 1996; Zhong et al., 2000). Conservation of mass, momentum (which together define the steady state flow field) and conservation of energy (which defines a time-dependent temperature field) are solved assuming an incompressible flow and adopting the Boussinesq approximation, with an a posteriori adiabatic temperature correction of 0.5 K/km. Tracking of material properties and water content is performed using a second-order Runge–Kutta tracer particle technique. Further details on the governing equations and associated numerical methods are described in van Hunen and Allen (2011). For each tracer, the stable mineral phases are calculated using a Gibbs free energy minimization strategy (Connolly, 2005, 2009), see Section 2.2 below. Initially, water is only present within the slab on the left hand side of the model. It is subsequently carried deeper within the slab until dehydration occurs. If, according to Gibbs energy minimization, free water is one of the stable phases, it is collected for all tracers in each element, moved to and distributed over the tracers in the element above (Gerya et al., 2002; Arcay et al., 2005), where it is added to the composition to affect the stable mineral phases. This approach assumes that water percolation in the mantle occurs on time scales much shorter than mantle convection. We run our simulations long enough to reach a quasi-steady-state condition in the slab in which the dehydration processes do not change anymore with time.

The computational domain is 300 km deep and 600 km wide, with a grid resolution of about 0.6×0.6 km^2 (Fig. 1). We use a commonly applied model setup of a kinematically described subducting slab (e.g. Syracuse et al., 2010). Since slab deformation is not of first-order importance in this study, we use a straight slab (as e.g. in van Keken et al., 2008) subducting under a 30° angle with a constant velocity of 5 cm/yr. To allow subduction, a 4.5 km thick weak fault zone (with an effective, relatively low viscosity $\eta = 10^{21}$ Pa s) is imposed between the subducting and overriding plate. The temperature field is first computed in a model in which the subduction of oceanic lithosphere with a given age evolves until it reaches a quasi-steady-state condition. This thermal structure is subsequently used as the initial temperature field for further

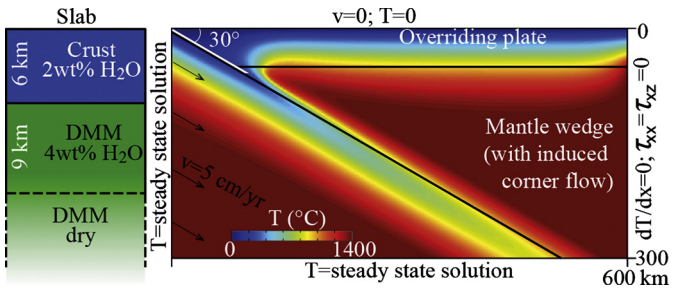

Fig. 1. Schematic representation of the computational model setup. A slab with constant dip angle enters the computational domain from the left with a fixed temperature (half-space cooling temperature for given plate age) and fixed velocity and leaves it from the bottom. The top boundary conditions are no-slip and zero surface temperature (0 °C). Stress free outflow and zero diffusional heat flow are the boundary conditions on the right-hand side boundary. The slab consists of a 6 km thick hydrated crust (2 wt% H_2O) and a 9 km underlying DMM mantle (either dry or hydrated to 4 wt% H_2O), and a dry DMM mantle underneath. The grey area between the plates shows the weak fault zone.

Table 1
Symbols, units and default model parameters.

Parameters	Symbols (unit)	Value
Temperature	T_{abs} (K)	–
Mantle potential temperature	T_m (K)	1623
Reference mantle viscosity	η_0 (Pa s)	10^{21}
Maximum mantle viscosity	η_{mm} (Pa s)	10^{24}
Lithosphere viscosity	η_l (Pa s)	10^{26}
Weak zone viscosity	η_w (Pa s)	10^{21}
Gas constant	R (J/mol/K)	8.3
Activation energy	E (kJ/mol)	360
Plate velocity	v (cm/yr)	5
Mesh resolution	km^2	0.6×0.6

model calculations. Temperature is prescribed at the top and inflow boundary, while a zero conductive heat flux applies on the right and bottom boundaries. The velocity boundary conditions are no-slip at the top, imposed velocity at the slab in- and outflow boundary, and stress free flow at the right boundary. The mantle wedge flow is kinematically driven by the slab descent. We use a temperature-dependent rheology in the mantle wedge, in which the deformation is accommodated by diffusion creep (Table 1):

$$\eta_{diff} = \eta_0 \exp\left(\frac{E}{RT_{abs}} - \frac{E}{RT_m}\right)$$

Plates have a constant viscosity of 10^{26} Pa s. A maximum viscosity of 10^{24} Pa s is imposed for the mantle wedge. The obtained slab temperatures in our models are within the range of those proposed for such conditions (Gerya et al., 2002; van Keken et al., 2008; Syracuse et al., 2010). At each time step, which corresponds to about 3000 yrs, the obtained pressure, temperature and composition are used to compute the stable phases from the thermodynamic database (see below).

2.2. Thermodynamical model set-up

We investigate the petrological processes involved in intermediate-to-warm subduction zones using compositions for the crust and mantle lithologies that have been widely used previously, and that can be considered as benchmark compositions. In these models, the slab crust is a 6-km compositionally homogeneous hydrated (2 wt% H_2O) layer representing the bulk of the igneous oceanic crust (sample LTBC, Poli, 1993; Poli and Schmidt, 1995; Schmidt and Poli, 1998). Underneath is a depleted lithospheric mantle (DMM, Workman and Hart, 2005) with or without a hydrated shallow part (9 km, with 4 wt% H_2O) representing serpentinized mantle. Such slab compositions are considered

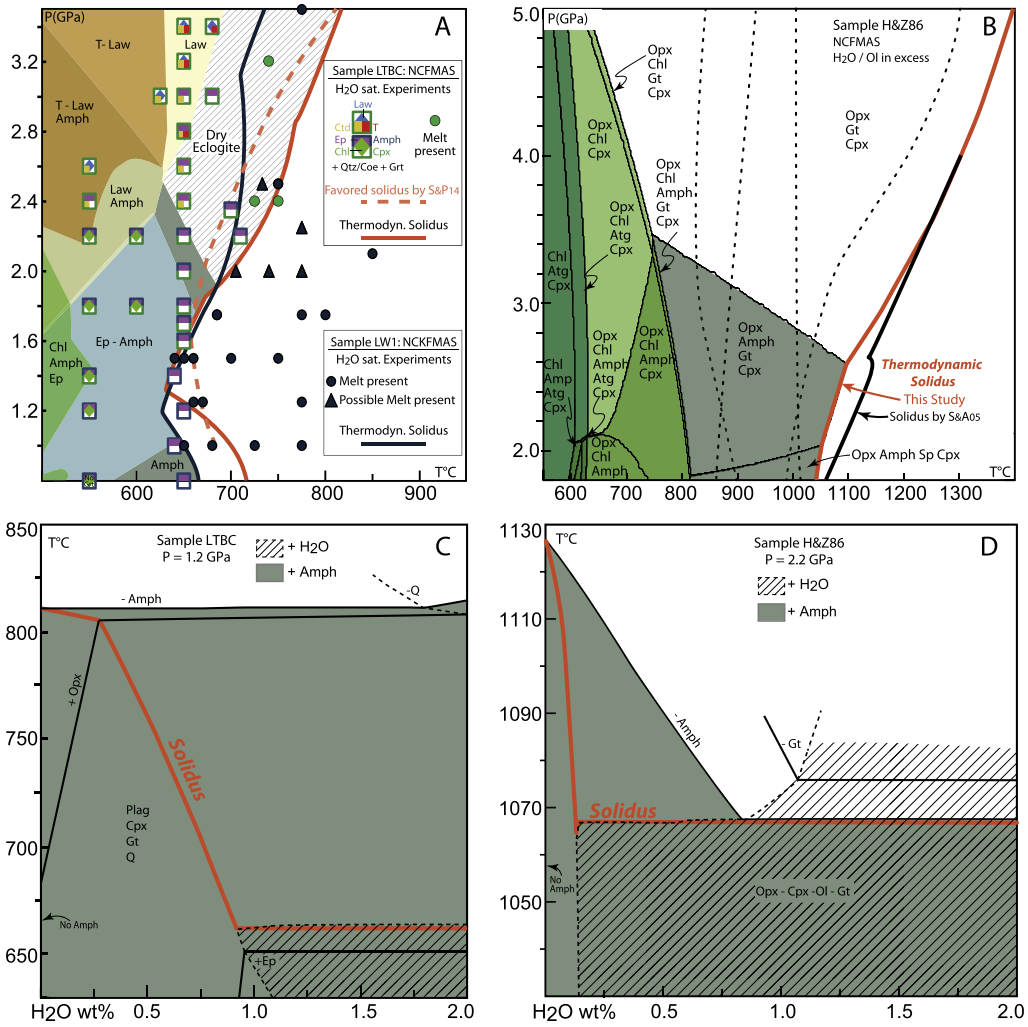

Fig. 2. Calculated pressure–temperature (P–T) and temperature–water content (T–X) diagrams in the NCFMASH closed system. A) P–T space showing the fields of stability of hydrous phases calculated for sample LTBC, with 2 wt% H_2O. Dry eclogites = Cpx + Grt. SiO_2 is in excess. Also shown are experiments on LTBC where melt is present, and the favored solidus from Schmidt and Poli (2014) (S&P14). A comparison of our thermodynamic solidus in the NCKFMASH system with the one obtained experimentally for sample "1" of Lambert and Wyllie (1972) is shown in black. Phengite solid-solution from Holland and Powell (1998) added to account for potassium. B) P–T diagram calculated for the primitive mantle composition of Hart and Zindler (1986) in water saturated conditions, showing the location of our thermodynamic solidus, compared to the one of Smith and Asimow (2005) (S&A05). For comparison, parameterized and experimentally derived solidi are shown as dotted lines: from left to right at 4 GPa: Till et al. (2012); Katz et al. (2003); Kawamoto and Holloway (1997); Green et al. (2010). C) T–X section of crustal sample LTBC at 1.2 GPa showing the trace of our solidus as a function of water content. D) T–X section of the primitive mantle composition showing the trace of our solidus as a function of water content. Amph = Amphibole; Atg = Antigorite; Chl = Chlorite; Ctd = Chloritoid; Ep = Epidote; Gt = Garnet; Law = Lawsonite; T = Talc; Q = quartz; Ol = Olivine; Opx = Orthopyroxene; Cpx = Clinopyroxene, Sp = Spinel.

representative of a subducting slab (e.g. Connolly, 2005; Hacker, 2008). The mantle wedge is represented by a primitive mantle composition (Hart and Zindler, 1986). The chemical space is modeled in the Na_2O–CaO–FeO–MgO–Al_2O_3–SiO_2–H_2O (NCFMASH) system. Our choices of solid-solutions reproduce fairly well the sub-solidus crustal and mantle parageneses (Fig. 2A, B) (Thompson and Ellis, 1994; Fumagalli and Poli, 2005). Minerals and solid solutions model data are from Holland and Powell (1998) except for amphibole (Wei and Powell, 2003; White et al., 2003), spinel (Jamieson and Roeder, 1984) and plagioclase (Newton et al., 1980). The thermodynamic behavior of water is dictated by the equation of state of Holland and Powell (1991). For melt, the solid solution used is from White et al. (2001), except that the Gibbs free energy corrections (DQF) for the magnesium and iron component (foL and faL) have not been taken into account; and that a pressure (bar) dependency of −2.5 has been added to the DQF of the main aluminum component (silL) that was implemented in the solid solution by White et al. (2007) (DQFsilL kJ/mol: −10; 0; −2.5). These modifications are intended to use the original interaction energy involving foL and faL and to better represent the solidus and melting reactions at higher pressure (in the systems considered here). Our choice of solid solutions reproduce the solidus and melting reaction in water-saturated and unsaturated conditions for both crustal and mantle compositions (Fig. 2). Furthermore, although our melt–solid solution predicts melting for the mantle at higher temperatures than what has been experimentally determined, it is in line with other thermodynamic solidi (Smith and Asimow, 2005). Our study intends to only constrain the presence or absence of melt and the melting reactions as a function of water content, and not any subsequent melt compositional evolution. Once formed, melts are not moved, implying that chemical mixing and melt–rock reaction during percolation are not considered. Therefore, we do not use the thermodynamic calculations to constrain melt volume or composition. When melt is present, the melt composition is discussed via experimental results.

We present results for three different models: those for a 40-Myr old slab to illustrate the various dehydration reactions; and two models for a comparatively hot slab of 5 Myr of age, one with

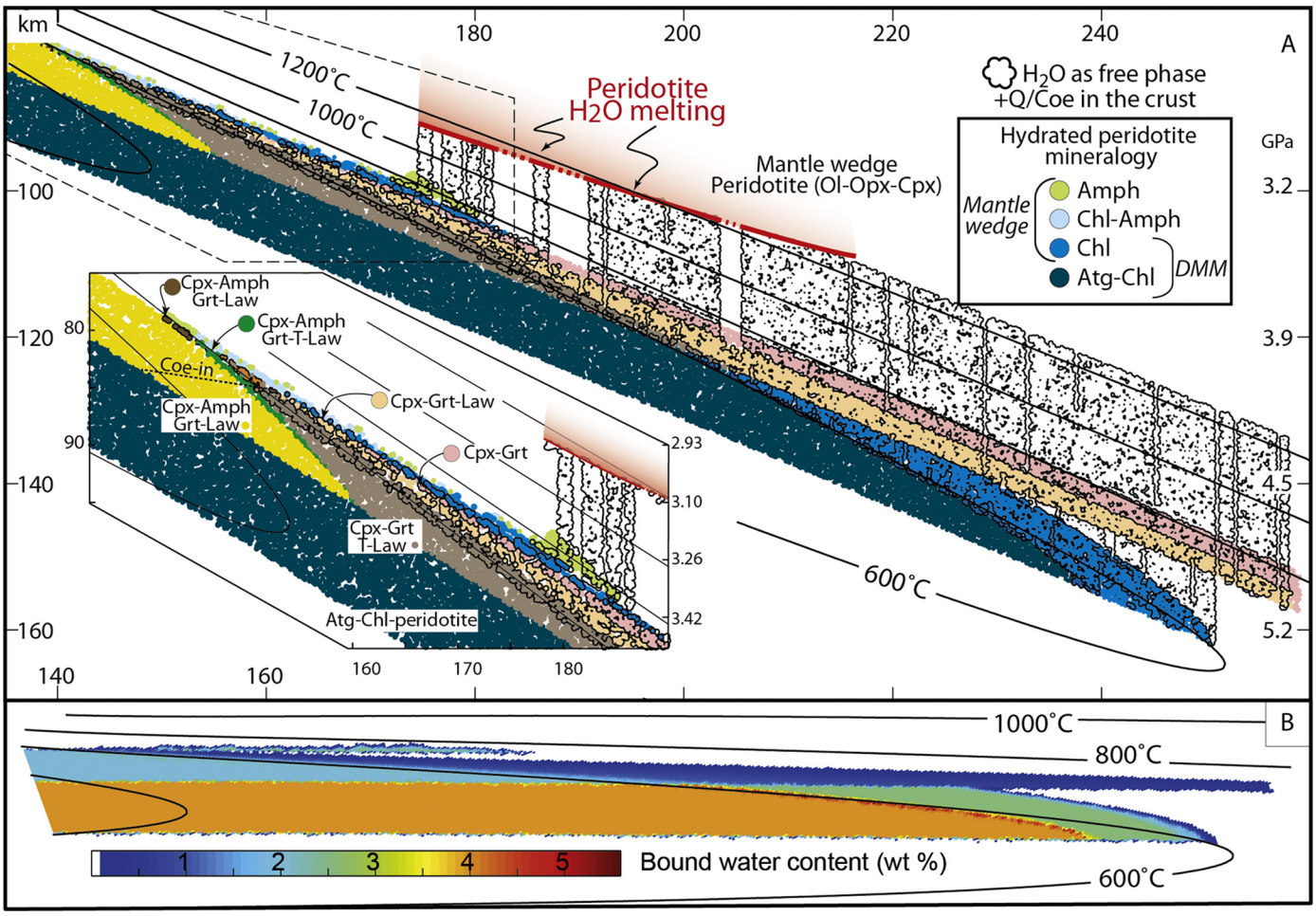

Fig. 3. Paragenetic map of a 40-Myr old subducting slab. A) Colored symbols show the different parageneses. Where circled in black, H_2O is present as a free phase. Mantle wedge peridotite and dry slab mantle are left white. Peridotite = Ol + Opx + Cpx ± Spinel/Garnet (transition omitted for clarity). Quartz/coesite transition = Coe-in dashed line only shown in the inset. Abbreviations as in Fig. 2. B) Bound water content within the slab.

and one without a hydrated mantle lithosphere. These last two models enable us to characterize the different melting reactions and to assess how dehydration of slab mantle lithosphere influences melting of slab crust and mantle wedge.

3. A paragenetic map of an ordinary slab

The dehydration/rehydration pattern for a thermally rather ordinary 40-Myr old subducting slab is shown in Fig. 3. At depths >80 km, the hydrated part of the slab mantle has been transformed into an Atg (antigorite)-Chl (chlorite) bearing peridotite, under isochemical conditions, which remains stable until it undergoes two major dehydration events related to Atg and Chl breakdown. These two temperature-dependent reactions cause the mantle part of the slab to undergo complete devolatilization along a wide depth range, nearly parallel to the 620 °C isotherm, from ~130 km to 160 km (4–5 GPa) thus being a potential source of fluid for the overlying crust and mantle wedge. Atg breakdown diminishes the water content of the descending mantle from 4 to ~2.5 wt% H_2O, whereas the disappearance of Chl leaves a fully dried oceanic mantle (Fig. 3B). In a cooler scenario (e.g. older slab), the mantle part of the slab would easily store a large amount of water due to the formation of phase-A which is not achieved in a 40 Myr-old slab (e.g. Thompson, 1992; Fumagalli and Poli, 2005; van Keken et al., 2011; Magni et al., 2014).

The crustal part of the slab experiences a more complex metamorphic history, which transforms the basaltic crust from Amph (amphibole)–Cpx (clinopyroxene)–Grt (garnet)–Ky (Kyanite)–Q (quartz) at 50 km (1.6 GPa, 200 °C) to an eclogitic paragenesis composed of Cpx–Grt–Law (lawsonite)–T (talc)–Coe (coesite) near 90 km depth (2.9 GPa; 590 °C), decreasing the water content by nearly 1 wt% H_2O (Fig. 3B). From there on, talc and Law breakdown reactions dictate the dehydration pattern of the slab crust. Talc breakdown, nearly parallel to the 600 °C isotherm, is the first reaction to liberate water, which becomes a free phase traveling through the overlying H_2O saturated Law-eclogites that can only hold about 1 wt% H_2O. Beyond 120 km depth, talc is not stable and the slab crust is a double layer of Law–Cpx–Grt eclogite overlain by Cpx–Grt eclogites. This depth also corresponds to the beginning of the slab mantle dehydration, leading to the presence of free water originating from the dehydrating slab mantle, in the double layered slab crust. At depth >150 km, Law breakdown in the crust allows small H_2O amounts to be delivered to the overlying mantle wedge. The slab crust further transforms entirely to dry Cpx–Grt eclogites.

In the mantle wedge, hydrous phases appear as a result of crustal dehydration. Chl and Amph are stable in the peridotite above the first water release reactions between 80 and 90 km depth where Amph, and later talc, breaks down in the crust. This thin layer of hydrated peridotite (~2 wt% H_2O) becomes slightly thicker near 100 km depth. Between 100 and 105 km depth, the water supply to the overlying mantle wedge is maximized by breakdown of both Amph in the hydrated mantle wedge layer and talc in the slab crust. H_2O becomes available as a free phase

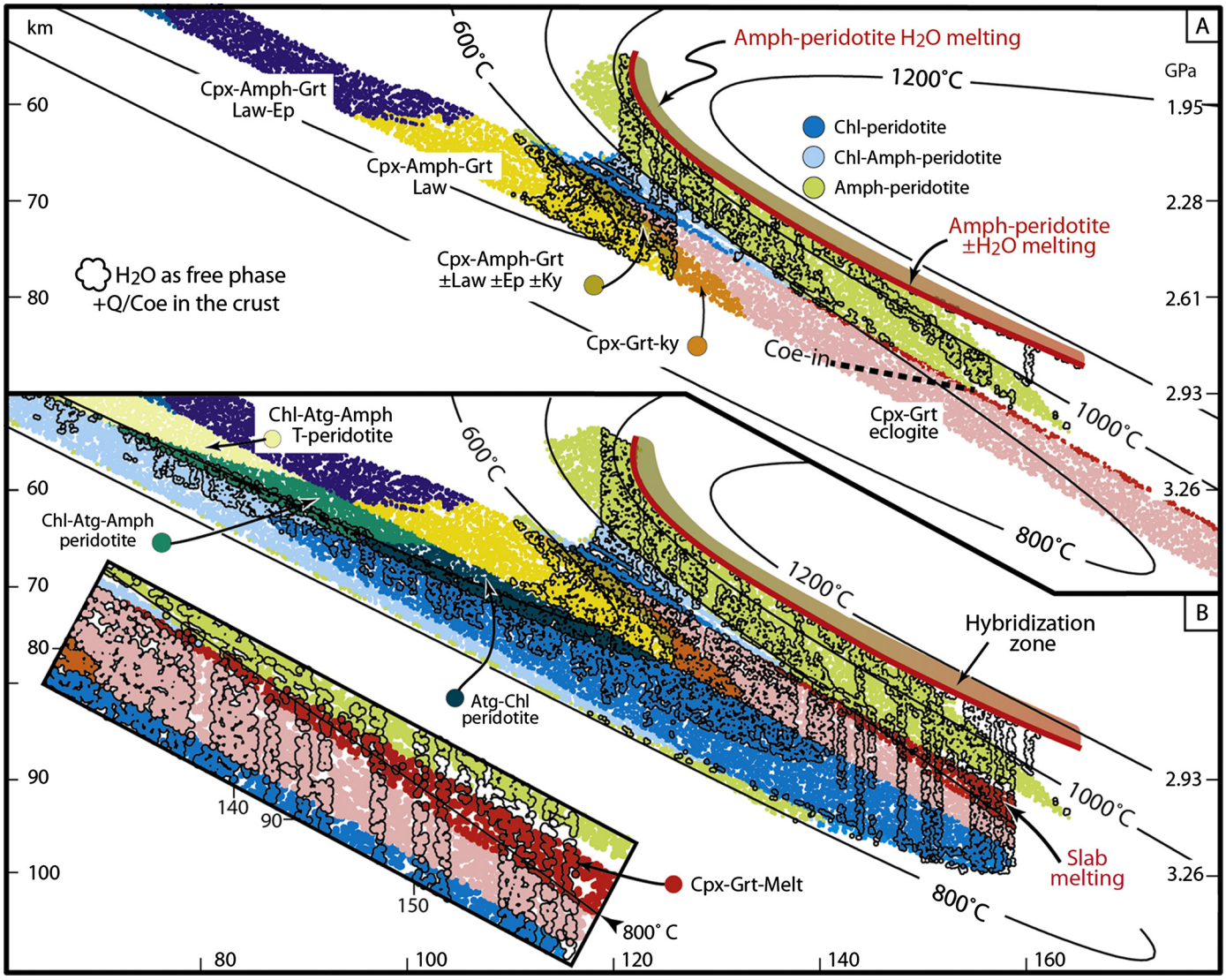

Fig. 4. Paragenetic map of a 5-Myr old subducting slab with A) an initially dry mantle lithosphere, and B) an initially hydrated mantle lithosphere. Because melt is not removed once formed, a thin layer of melt develop in A (see text). The inset in B is a zoom-in of the slab melting region. Abbreviations as in Fig. 2.

around 95 km depth within the mantle wedge and then percolates upwards to ~90 km, where it allows the Grt-peridotite to melt in water-present conditions. This is where mantle melting would be maximized in our model. At greater depth, once talc is exhausted, two reactions control the supply of water to the mantle wedge: Law breakdown in the crust and Chl breakdown in the slab mantle.

4. Paragenetic maps of warm slabs

Slab melting is often attributed to high temperatures in a (young) subducting slab, and in the next paragraphs we investigate such melting process by simulating the subduction of a young lithosphere. We intend to constrain the consequences of dehydration, and the process through which slab melting can be achieved. In Fig. 4A we first show a 5-Myr old slab model that does not have a hydrated mantle. Although it is unlikely that the slab mantle is not hydrated whereas the crust is, this situation provides insight in the viability of slab dehydration melting (without excess water) alone. A second model (Fig. 4B), in which a hydrated mantle layer is added to the young slab, addresses a more realistic, more complex scenario of crustal de- and rehydration, and consequences for slab and mantle melting, which then constrains the role of the released metamorphic fluid.

4.1. The dry slab mantle case

Crust in a young slab experiences complete dehydration at shallow depth, in a small P–T window, through a series of reactions from a Cpx–Amph–Gt–Law–Q assemblage at 65 km to a dry eclogite made of Cpx–Gt–Q at ~75 km (Fig. 4A). Because water-bearing minerals and free water are then absent, the crust does not melt. This illustrates an important point: even in a very warm case, dehydration precedes melting, thus dehydration melting is not operative.

Due to dehydration of slab crust at shallow depths, a thick hydrated peridotite layer forms in the overlying mantle wedge (Fig. 4A). Consequently, water saturated melting of Amph-peridotite occur near 2 GPa, where the mantle is continuously supplied with slab metamorphic fluids. The hydrated peridotite is dragged down by corner flow and melting occurs mainly through Amph dehydration between ~2.2 and 2.9 GPa. Therefore, our model shows that mantle melting reactions are contrastingly different from a 40 Myr old slab: they involve Amph-peridotite in water-present and water-absent conditions, occurring over a shallow, but wide

pressure range (2.0–2.9 GPa), feeding the overriding plate with primitive mantle melts.

Fig. 4A further shows that crustal melt is formed at the interface between the dry slab crust eclogites and the dehydrating Amph-peridotite of the wedge because of the presence of free water from the dehydrating Amph-peridotite. Although insignificant and only occurring at the slab–mantle interface, it illustrates the effect of free water on dry eclogites above their water-saturated solidus (Laurie et al., 2013).

4.2. The wet mantle slab case

In the presence of an underlying hydrated slab mantle, the crust dehydrates as quickly as in the above scenario, but compared to the 40 Myr-old slab case (Fig. 3), the lower portion of the hydrated, relatively hot slab mantle layer dehydrates first (Fig. 4B) because the 600 °C isotherm is contained within the hydrated part of the slab. Between 55 and 72 km depth, on the high temperature side of the 600 °C isotherm, the successive Amph and Chl breakdown liberates free water, hydrating the cooler slab mantle above. From ~72 km, where the 600 °C isotherm crosses the slab crust–mantle interface, to 100 km depth, the successive Atg and Chl breakdown delivers free water to the overlying crust. Near 75 km depth, this free water combines with the water freed from the dehydrating crust and contributes to hydrate the overlying mantle wedge to a greater extend. Deeper, the dry eclogitic crust becomes flushed by the water liberated from the Chl-breakdown reaction occurring in the slab mantle, and is able to melt in water-saturated conditions (Grt + Cpx ± Coe + H_2O melting reaction). As discussed by e.g. Laurie and Stevens (2012), this produces dacitic melts comparable to low X_{Mg} high-silica adakites. In this case, the crust melts through a similar mechanism as the mantle wedge does in a "normal" subduction zone, i.e. through the supply of metamorphic water from deeper slab dehydration, a process suggested to occur in many subduction zone (Spandler and Pirard, 2013).

Although our model predicts that the crust of a 5 Myr-old slab will melt, it also predicts, like in the cases discussed above, extensive mantle wedge melting. Hence, significant melting is occurring in the wedge above the region where the slab melts could be extracted.

5. Discussion

5.1. Assessing solidus uncertainties

For the crust, our solidus is close to the experimental data. Nevertheless, The P–T path of the 5 Myr young slabs would cross the water-saturated solidus near 2.3 GPa and 700 °C, where the position of the solidus and the possible parageneses are somewhat uncertain (Fig. 2). If any Amph or Ep (epidote) were stable, Ep-out dehydration melting would produce very little melt, and since these conditions approach the upper pressure limit of Amph stability, a limited amount of Amph-out dehydration melting would also occur (Poli and Schmidt, 1995). This illustrates that our models predict, within experimental uncertainties, the conditions for slab melting.

For the mantle wedge, a wide range of water-saturated solidi have been determined experimentally and thermodynamically (see Fig. 2). Our water-saturated solidus is close to the pHMELTS model of Smith and Asimow (2005), both being on the high temperature end-member compared to experimentally derived solidus (Fig. 2B). The use of our melt solid solution has the advantage of being derived using a single database that is suitable for the whole range of modeled compositions, and do not rely on an externally calibrated curve. Nevertheless, all determined solidi (including the one presented here) for water bearing mantle involve a hydrous phase and/or free H_2O at the onset of melting. For most studies, amphibole is the hydrous phase to be present, and its presence is mainly pressure dependent, varying for its upper stability limit from 2 to 3 GPa, free water being present above (e.g. Millhollen et al., 1974; Niida and Green, 1999). Chlorite-present melting, instead of free water, has also been shown to be possible (Grove et al., 2006; Till et al., 2012), but thermodynamic calculations fail to reproduce such chlorite–melt relationships. Hence, in the case of the 40 Myr slab model, where the first fluid release occurs deeper than 3 GPa, the use of most experimentally derived solidi would bring the location of the solidus closer to the slab–mantle interface, but would involve the same melting reaction (i.e. dry peridotite + H_2O = melt). Similarly, for the case of the very young slab, a lower-T mantle wedge solidus would affect the depth at which the solidus is reached: the location of the solidus would be closer to the slab-mantle interface. Considering that all fluid release reactions occur between 2.2 and 2.9 GPa, where Amph is present, the melting reactions would still be the same as those for a higher-T solidus.

Therefore, even if solidus temperatures were lower than the thermodynamically determined ones, the subduction of a young warm slab would still result in significant mantle wedge melting, but occurring at shallower depths between 2 and 2.9 GPa.

5.2. Expected magmatic output of warm subduction zones

So, in contrast with colder slabs, warm subduction zones show a significant amount of mantle wedge melts produced in water saturated conditions at shallow depth (~2 GPa), where Amph is present. In such conditions, these primitive mantle melts will approach a high X_{Mg} andesitic composition (e.g. Mysen and Boettcher, 1975; Hirose, 1997), which is notably different from those expected in the 40 Ma old slab models (Gaetani and Grove, 1998; Ulmer, 2001). Importantly, the mantle melts formed near this depth (60–70 km), en route to the overriding lithosphere, will not travel through the hot core of the wedge (Fig. 4), and will therefore not be subject to flux melting (Grove et al., 2006). Instead, these mantle melts will rapidly impinge the normal gradient of the overriding plate (i.e. decreasing temperature with decreasing pressure) and will be readily subject to fractionation. In such conditions the fractionation sequence of these water-rich melts involve the appearance of garnet at the liquidus (Muntener et al., 2001; Alonso-Perez et al., 2009), forming derivative liquids showing an adakitic signature (e.g. Macpherson et al., 2006; Alonso-Perez et al., 2009).

The siliceous slab melts are produced in the warm subduction zone via advection of metamorphic fluids through the slab crust and have an "adakitic" signature. These melts would extensively react with the peridotite present above the slab. Experimental results show that the reactions between high-silica low X_{Mg} slab melt and peridotite produce garnet-pyroxenites (± Phlogopite ± H_2O, Sekine and Wyllie, 1982) and reacted liquids that remain silica-rich but with much higher X_{Mg}, difficult to differentiate from mantle-derived high X_{Mg} Andesite (Sekine and Wyllie, 1982; Rapp et al., 1999). Alternatively, amphiboles and orthopyroxene can also be solid reaction products (Sen and Dunn, 1995) of slab melt/peridotite interaction. The fate of the remaining liquid and residue, as well as the reaction process is difficult to predict, considering the petrological complexity above the slab melting region. Our models do not account for this complexity because melts are not moved once formed, but they show that the mantle wedge is melting above the slab melting region (~2.9 GPa). Therefore, any slab melts that may survive the reaction with the Amph-peridotite would encounter a region of the wedge where the mantle is potentially melting, leading to a hybridization of mantle derived and mantle-reacted slab melts (hybridization zone, Fig. 4B). Importantly, these melts will have to go through the hot core of the

wedge, where they will be subject to further reaction at increasing temperature. Despite the complexity of the slab melt–mantle reactions, the discussion above implies that the contribution of slab melts to the overriding plate is very limited. Instead, our models show that the overriding plate is largely fed with primitive Amph-bearing mantle melts produced at 2 GPa that did not travel through the hot core of the mantle wedge.

6. Conclusions

We quantified the petrological processes in a warm subduction system and the feasibility of oceanic crust slab melting. Melting of the oceanic crust is often emphasized to occur in warm subduction zones and to be controlled by the slab surface temperature, but we demonstrate that the hydration state of the slab is equally paramount for the generation of oceanic crust slab melts. We show that a high temperature gradient along the slab does not induce significant slab melting, because the crust in a warm slab devolatilizes completely at shallow depth, thereby suppressing dehydration melting potential. Significant slab crust melting is only feasible through the reaction of dry eclogite with free water derived from the deeper portions of the slab (e.g. Laurie and Stevens, 2012). These results emphasize the importance of the hydration state of the slab, and our need to better constrain the hydration mechanism at the ridge and during bending (e.g. Ranero and Sallares, 2004; Iyer et al., 2012; Faccenda, 2014) for extrapolating the melting potential of the descending crust.

Although conditions can be met to produce melts within the oceanic crust, our models demonstrate that the shallow slab dehydration also produces a thick hydrated mantle wedge, which generates partial melts from Amph-peridotite over a wide range of pressures at shallow depth. These melts will have a contrasting composition compared to melts formed above colder slabs, and will provide a challenging environment for the survival of pristine slab melts. Moreover, these parental mantle melts will not be transferred through the hot mantle wedge core, and will most likely fractionate garnet and amphibole, giving an adakitic flavor to their descendants. Just like for cold subduction zones, the mantle wedge is also the main supplier of melt for the overriding plate in a warm subduction regime.

Acknowledgements

This study was supported by the European Research Council (ERC StG 279828). LK acknowledges support from the Marie Curie Initial Training Network TOPOMOD (grant number 264517). The authors are grateful for discussions with J.A.D. Connolly, J.-F. Moyen, C. Macpherson, and J. Davidson. We further thank two anonymous reviewers for their comments and suggestions that greatly improved the manuscript.

References

Alonso-Perez, R., Muntener, O., Ulmer, P., 2009. Igneous garnet and amphibole fractionation in the roots of island arcs: experimental constraints on andesitic liquids. Contrib. Mineral. Petrol. 157, 541–558.

Arcay, D., Tric, E., Doin, M.P., 2005. Numerical simulations of subduction zones: effect of slab dehydration on the mantle wedge dynamics. Phys. Earth Planet. Inter. 149, 133–153.

Arculus, R., 1981. Island arc magmatism in relation to the evolution of the crust and mantle. Tectonophysics 75, 113–133.

Atherton, M.P., Petford, N., 1993. Generation of sodium-rich magmas from newly underplated basaltic crust. Nature 362, 144–146.

Connolly, J.A.D., 2005. Computation of phase equilibria by linear programming: a tool for geodynamic modeling and its application to subduction zone decarbonation. Earth Planet. Sci. Lett. 236, 524–541.

Connolly, J.A.D., 2009. The geodynamic equation of state: what and how. Geochem. Geophys. Geosyst. 10, Q10014.

Defant, M.J., Drummond, M.S., 1990. Derivation of some modern arc magmas by melting of young subducted lithosphere. Nature 347, 662–665.

Faccenda, M., 2014. Water in the slab: a trilogy. Tectonophysics 614, 1–30.

Fumagalli, P., Poli, S., 2005. Experimentally determined phase relations in hydrous peridotites to 6 · 5 GPa and their consequences on the dynamics of subduction zones. J. Petrol. 46, 555–578.

Gaetani, G.A., Grove, T.L., 1998. The influence of water on melting of mantle peridotite. Contrib. Mineral. Petrol. 131, 323–346.

Gerya, T.V., Stockhert, B., Perchuk, A.L., 2002. Exhumation of high-pressure metamorphic rocks in a subduction channel: a numerical simulation. Tectonics 21.

Green, D.H., Hibberson, W.O., Kovacs, I., Rosenthal, A., 2010. Water and its influence on the lithosphere–asthenosphere boundary. Nature 467, 448–451.

Grove, T.L., Chatterjee, N., Parman, S.W., Medard, E., 2006. The influence of H_2O on mantle wedge melting. Earth Planet. Sci. Lett. 249, 74–89.

Hacker, B.R., 2008. H_2O subduction beyond arcs. Geochemistry Geophysics Geosystems 9.

Hart, S.R., Zindler, A., 1986. In search of a bulk-Earth composition. Chem. Geol. 57, 247–267.

Hirose, K., 1997. Melting experiments on lherzolite KLB-1 under hydrous conditions and generation of high-magnesian andesitic melts. Geology 25, 42–44.

Holland, T., Powell, R., 1991. A Compensated-Redlich–Kwong (CORK) equation for volumes and fugacities of CO_2 and H_2O in the range 1 bar to 50 kbar and 100–1600 °C. Contrib. Mineral. Petrol. 109, 265–273.

Holland, T.J.B., Powell, R., 1998. An internally consistent thermodynamic data set for phases of petrological interest. J. Metamorph. Geol. 16, 309–343.

Iwamori, H., 1998. Transportation of H_2O and melting in subduction zones. Earth Planet. Sci. Lett. 160, 65–80.

Iyer, K., Rüpke, L.H., Phipps Morgan, J., Grevemeyer, I., 2012. Controls of faulting and reaction kinetics on serpentinization and double Benioff zones. Geochem. Geophys. Geosyst. 13.

Jamieson, H.E., Roeder, P.L., 1984. The distribution of Mg and Fe 2+ between olivine and spinel at 1300 °C. Am. Mineral. 69, 283–291.

Katz, R.F., Spiegelman, M., Langmuir, C.H., 2003. A new parameterization of hydrous mantle melting. Geochem. Geophys. Geosyst. 4, 1073.

Kawamoto, T., Holloway, J.R., 1997. Melting temperature and partial melt chemistry of H_2O-saturated mantle peridotite to 11 gigapascals. Science 276, 240–243.

Kay, R.W., 1978. Aleutian magnesian andesites: melts from subducted Pacific ocean crust. J. Volcanol. Geotherm. Res. 4, 117–132.

Lambert, I.B., Wyllie, P.J., 1972. Melting of gabbro (quartz eclogite) with excess water to 35 kilobars, with geological applications. J. Geol. 80, 693–708.

Laurie, A., Stevens, G., 2012. Water-present eclogite melting to produce Earth's early felsic crust. Chem. Geol. 314–317, 83–95.

Laurie, A., Stevens, G., van Hunen, J., 2013. The end of continental growth by TTG magmatism. Terra Nova 25, 130–136.

Macpherson, C.G., Dreher, S.T., Thirlwall, M.F., 2006. Adakites without slab melting: high pressure differentiation of island arc magma, Mindanao, the Philippines. Earth Planet. Sci. Lett. 243, 581–593.

Magni, V., Bouilhol, P., van Hunen, J., 2014. Deep water recycling through time. Geochem. Geophys. Geosyst. 15. http://dx.doi.org/10.1002/2014GC005525.

Martin, H., 1999. Adakitic magmas: modern analogues of Archaean granitoids. Lithos 46, 411–429.

Millhollen, G.L., Irving, A.J., Wyllie, P.J., 1974. Melting interval of peridotite with 5.7 per cent water to 30 kilobars. J. Geol. 82, 575–587.

Moresi, L., Gurnis, M., 1996. Constraints on the lateral strength of slabs from three-dimensional dynamic flow models. Earth Planet. Sci. Lett. 138, 15–28.

Moyen, J.-F., 2009. High Sr/Y and La/Yb ratios: the meaning of the "adakitic signature". Lithos 112, 556–574.

Muntener, O., Kelemen, P.B., Grove, T.L., 2001. The role of H_2O during crystallization of primitive arc magmas under uppermost mantle conditions and genesis of igneous pyroxenites: an experimental study. Contrib. Mineral. Petrol. 141, 643–658.

Mysen, B.O., Boettcher, A., 1975. Melting of a hydrous mantle: II. Geochemistry of crystals and liquids formed by anatexis of mantle peridotite at high pressures and high temperatures as a function of controlled activities of water, hydrogen, and carbon dioxide. J. Petrol. 16, 549–593.

Newton, R.C., Charlu, T.V., Kleppa, O.J., 1980. Thermochemistry of the high structural state plagioclases. Geochim. Cosmochim. Acta 44, 933–941.

Niida, K., Green, D.H., 1999. Stability and chemical composition of pargasitic amphibole in MORB pyrolite under upper mantle conditions. Contrib. Mineral. Petrol. 135, 18–40.

Poli, S., 1993. The amphibolite–eclogite transformation, an experimental study on basalt. Am. J. Sci. 293, 1061–1107.

Poli, S., Schmidt, M.W., 1995. H_2O transport and release in subduction zones: experimental constraints on basaltic and andesitic systems. J. Geophys. Res., Solid Earth 100, 22299–22314.

Ranero, C., Sallares, V., 2004. Geophysical evidence for hydration of the crust and mantle of the Nazca plate during bending at the north Chile trench. Geology 32, 549–552.

Rapp, R.P., Shimizu, N., Norman, M.D., Applegate, G.S., 1999. Reaction between slab-derived melts and peridotite in the mantle wedge: experimental constraints at 3.8 GPa. Chem. Geol. 160, 335–356.

Rapp, R.P., Watson, E.B., Miller, C.F., 1991. Partial melting of amphibolite/eclogite and the origin of Archean trondhjemites and tonalites. Precambrian Res. 51, 1–25.
Ringwood, A.E., 1974. The petrological evolution of island arc systems. J. Geol. Soc. Lond. 130, 183–204.
Rüpke, L.H., Morgan, J.P., Hort, M., Connolly, J.A., 2004. Serpentine and the subduction zone water cycle. Earth Planet. Sci. Lett. 223, 17–34.
Schmidt, M.W., Poli, S., 1998. Experimentally based water budgets for dehydrating slabs and consequences for arc magma generation. Earth Planet. Sci. Lett. 163, 361–379.
Schmidt, M.W., Poli, S., 2014. Devolatilization during subduction. In: Treatrise in Geochemistry, vol. 4, pp. 669–701.
Sekine, T., Wyllie, P.J., 1982. Synthetic systems for modeling hybridization between hydrous siliceous magmas and peridotite in subduction zones. J. Geol. 90, 734–741.
Sen, C., Dunn, T., 1995. Experimental modal metasomatism of a spinel lherzolite and the production of amphibole-bearing peridotite. Contrib. Mineral. Petrol. 119, 422–432.
Smith, P.M., Asimow, P.D., 2005. Adiabat_1ph: a new public front-end to the MELTS, pMELTS, and pHMELTS models. Geochem. Geophys. Geosyst. 6, Q02004.
Spandler, C., Pirard, C., 2013. Element recycling from subducting slabs to arc crust: a review. Lithos 170, 208–223.
Syracuse, E.M., van Keken, P.E., Abers, G.A., 2010. The global range of subduction zone thermal models. Phys. Earth Planet. Inter. 183, 73–90.
Tatsumi, Y., Kogiso, T., 1997. Trace element transport during dehydration processes in the subducted oceanic crust: 2. Origin of chemical and physical characteristics in arc magmatism. Earth Planet. Sci. Lett. 148, 207–221.
Taylor, S.R., McLennan, S.M., 1995. The geochemical evolution of the continental crust. Rev. Geophys. 33, 241–265.
Thompson, A.B., 1992. Water in the Earth's upper mantle. Nature 358, 295–302.
Thompson, A.B., Ellis, D.J., 1994. CaO + MgO + Al_2O_3 + SiO_2 + H_2O to 35 KB – amphibole, talc, and zoisite dehydration and melting reactions in the silica excess part of the system and their possible significance in subduction zones, amphibolite melting, and magma fractionation. Am. J. Sci. 294, 1229–1289.
Till, C., Grove, T., Withers, A., 2012. The beginnings of hydrous mantle wedge melting. Contrib. Mineral. Petrol. 163, 669–688.
Ulmer, P., 2001. Partial melting in the mantle wedge – the role of H_2O in the genesis of mantle-derived 'arc-related' magmas. Phys. Earth Planet. Inter. 127, 215–232.
Ulmer, P., Trommsdorff, V., 1995. Serpentine stability to mantle depths and subduction-related magmatism. Science 268, 858–861.
van Hunen, J., Allen, M.B., 2011. Continental collision and slab break-off: a comparison of 3-D numerical models with observations. Earth Planet. Sci. Lett. 302, 27–37.
van Keken, P.E., Currie, C., King, S.D., Behn, M.D., Cagnioncle, A., He, J., Katz, R.F., Lin, S.-C., Parmentier, E.M., Spiegelman, M., Wang, K., 2008. A community benchmark for subduction zone modeling. Phys. Earth Planet. Inter. 171, 187–197.
van Keken, P.E., Hacker, B.R., Syracuse, E.M., Abers, G.A., 2011. Subduction factory: 4. Depth-dependent flux of H_2O from subducting slabs worldwide. J. Geophys. Res., Solid Earth 116.
Wada, I., Behn, M.D., Shaw, A.M., 2012. Effects of heterogeneous hydration in the incoming plate, slab rehydration, and mantle wedge hydration on slab-derived H_2O flux in subduction zones. Earth Planet. Sci. Lett. 353–354, 60–71.
Wei, C., Powell, R., 2003. Phase relations in high-pressure metapelites in the system KFMASH (K_2O–FeO–MgO–Al_2O_3–SiO_2–H_2O) with application to natural rocks. Contrib. Mineral. Petrol. 145, 301–315.
White, R.W., Powell, R., Holland, T.J.B., 2001. Calculation of partial melting equilibria in the system Na_2O–CaO–K_2O–FeO–MgO–Al_2O_3–SiO_2–H_2O (NCKFMASH). J. Metamorph. Geol. 19, 139–153.
White, R.W., Powell, R., Holland, T.J.B., 2007. Progress relating to calculation of partial melting equilibria for metapelites. J. Metamorph. Geol. 25, 511–527.
White, R.W., Powell, R., Phillips, G.N., 2003. A mineral equilibria study of the hydrothermal alteration in mafic greenschist facies rocks at Kalgoorlie, Western Australia. J. Metamorph. Geol. 21, 455–468.
Workman, R.K., Hart, S.R., 2005. Major and trace element composition of the depleted MORB mantle (DMM). Earth Planet. Sci. Lett. 231, 53–72.
Zhong, S., Zuber, M.T., Moresi, L., Gurnis, M., 2000. Role of temperature-dependent viscosity and surface plates in spherical shell models of mantle convection. J. Geophys. Res., Solid Earth 105, 11063–11082.